THE JOURNAL OF PHYSICAL CHEMISTRY B

Article

pubs.acs.org/JPCB

Electron, Hole, Singlet, and Triplet Energy Transfer in Photoexcited Porphyrin-Naphthalenediimide Dyads

Oleksandr Yushchenko,[†] Rahul V. Hangarge,[‡] Sandra Mosquera-Vazquez,[†] Sheshanath V. Boshale,[§] and Eric Vauthey*[,†]

[†]Department of Physical Chemistry, University of Geneva, 30 quai Ernest-Ansermet, CH-1211 Geneva, 4, Switzerland

[‡]Department of Organic Chemistry, School of Chemical Sciences, North Maharashtra University, Jalgaon, 425 001 Maharashtra, India

[§]School of Applied Sciences, RMIT University, GPO Box 2476, Melbourne, Victoria 3001, Australia

Supporting Information

ABSTRACT: The excited-state dynamics of two molecular dyads, consisting of zinc (**1**) and free-base (**2**) porphyrin connected via a peptide linker to a core-substituted naphthalenediimide (NDI) have been investigated using optical spectroscopy. These dyads exhibit rich photophysics because of the large number of electronic excited states below 3 eV. In the case of **1** in apolar solvents, excitation energy transfer from the vibrationally hot singlet excited porphyrin to the NDI takes place with a 500 fs time constant. Electronic energy ends up in the NDI-localized triplet state, which decays to the ground state on a microsecond timescale. In polar solvents, ground-state recovery is faster by 5 orders of magnitude because of the occurrence of charge separation followed by recombination. On the other hand, excitation energy transfer in **2** takes place in the opposite direction, namely from the NDI to the porphyrin, which then undergoes intersystem crossing to the triplet state, followed by triplet energy transfer back to the NDI. Therefore, four distinct local electronic excited states are consecutively populated after excitation of the NDI unit of **2**, with the energy shuttling between the two ends of the dyad.

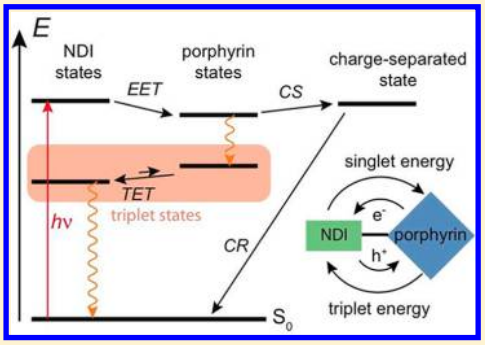

INTRODUCTION

Light absorption, excitation energy transfer (EET) and charge separation (CS) are crucial steps in natural photosynthesis,[1−3] which have to be optimized when designing efficient synthetic analogues.[4−11] Harnessing these processes in multichromophoric systems is also of the utmost importance for development in photonics, sensing and other applications based on photoactive molecular systems.[12−19]

Among the vast number of multichromophoric systems that have been reported so far, a large fraction are composed of identical chromophores arranged according to different motifs to favor excitation energy hopping while inhibiting aggregation and to act as antennae. Although most are based on porphyrins,[20−32] arrays with other chromophores, such as bodipy,[33−35] perylenediimides,[6,36−39] naphthalenediimides (NDI)[40−42] or triarylamines,[43] have also been reported. In polar environments, photoinduced symmetry-breaking CS between two identical units, usually perylenediimides and core-substituted NDIs,[44−47] can also take place, giving these arrays both antenna and reaction center functionality.

A significant number of systems composed of different chromophores absorbing in the visible region have also been reported,[48−54] the main motivation being to broaden the absorption spectrum of the array while creating an energy gradient to funnel the optical excitation toward a trap connected, for example, to an electron donor or acceptor.[55−61]

In such cases, the CS dynamics does not depend on the excitation wavelength, as the process usually takes place with the excitation on the same reaction partner. However, dyads where both the electron donor and the acceptor act as a chromophore are much less documented, and the excitation wavelength dependence (i.e., whether the donor or the acceptor is initially excited) of the CS dynamics has not often been investigated.[62−66] We have recently reported on the excited-state dynamics of a pentad consisting of a central NDI unit decorated at the core with four zinc (ZnP) or free-base porphyrins (FbP).[67] The CS dynamics in these arrays was found to depend on whether a porphyrin unit or the NDI core was initially excited. However, both pathways resulted in the same charge-separated state, and consequently, the ensuing charge recombination (CR) dynamics was independent of the excitation wavelength. An interesting feature of these arrays was that the lowest singlet excited-state was delocalized over the whole pentad.

We report here on our investigation of the excited-state dynamics of two bichromophoric systems (Chart 1) consisting of either a ZnP or FbP unit covalently bound via a peptide

Special Issue: John R. Miller and Marshall D. Newton Festschrift

Received: October 30, 2014
Revised: November 22, 2014
Published: November 24, 2014

DOI: 10.1021/jp5108685
J. Phys. Chem. B 2015, 119, 7308−7320

Chart 1. Structure of the Two Dyads

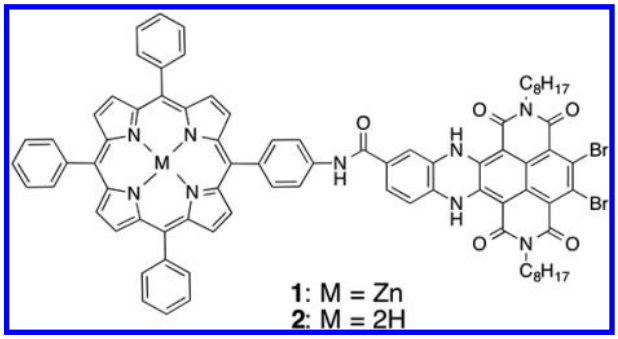

linkage to a hydroquinoxaline-substituted bromo-NDI (HNDI) in polar and apolar solvents using a combination of time-resolved spectroscopic techniques covering without interruption the femto- to microsecond timescales. Because of the peptide linkage, weak electronic coupling between the constituents was expected.[68,69] We will show that this is indeed the case and that, as a consequence, these dyads are characterized by a large number of electronic excited states, of both singlet and triplet multiplicity, below 3 eV. As a result, they exhibit very rich excited-state dynamics, involving, depending on the solvent and the nature of the porphyrin, electron, hole, singlet, and triplet excitation energy transfer and occurring on vastly different timescales.

EXPERIMENTAL SECTION

Sample. The synthesis of **1** and **2** is described in detail in the Supporting Information. In brief, the dyads were synthesized by the condensation of the 4,5-dibromo-2,7-dioctyl-1,3,6,8-tetraoxo-1,2,3,6,7,8,9,14-octahydro-[3,8]-phenanthrolino[1,10-abc]phenazine-11-carboxylic acid **3** with 5-(4-aminophenyl)-10,15,20-triphenylporphyrin **4** under argon atmosphere in the presence of 1-ethyl-3-(3-(dimethylamino)-propyl)carbodiimide and catalytic amount of 4-dimethylamino pyridine in dry DMF at room temperature for 12 h, giving crystalline purple solid of **2** in 91% yield. Finally, **1** was prepared by metalation of **2** with $Zn(OAc)_2$ in $CHCl_3$/MeOH (v/v,10:1) at room temperature, giving a purple solid. Compound **3** was prepared with a 31.4% yield according to literature procedure starting from naphthalene dianhydride in four steps.[70] Compound **4** was also prepared according to literature in two steps with a 54% yield.[71]

The solvents, toluene (Acros Organics, 99.5% for spectroscopy) and tetrahydrofuran (THF, Acros Organics, 99.5% for analysis), were used as received.

Steady-State Spectroscopy. Absorption spectra were measured on a Cary 50 spectrometer, whereas fluorescence emission and excitation spectra were recorded on a FluoroMax-4 (Horiba Scientific) fluorometer. All emission spectra were corrected for the wavelength-dependence sensitivity of the detector. The fluorescence quantum yields, Φ_f, were determined relatively to those of ZnP and FbP in benzene.

Time-Resolved Fluorescence. Fluorescence dynamics on the nanosecond timescale were measured using a time-correlated single photon counting (TCSPC) setup described in detail previously.[72,73] Excitation was performed at 395 nm using ~60 ps pulses at 10 MHz produced by a laser diode (Picoquant, LDH-P-C- 400B). The full width at half-maximum (fwhm) of the instrument response function (irf) was around 200 ps. Faster dynamics were investigated by fluorescence up-conversion (FU) using the same setup as in refs 74 and 75. Excitation was performed using 100 fs pulses centered at 420 nm produced by frequency, doubling the output of a Ti:sapphire oscillator (Spectra-Physics, Mai Tai). The pump intensity on the sample was around 5 $\mu J/cm^2$, and the fwhm of the irf was ca. 200 fs. The sample solutions were located in a 0.4 mm rotating cell and at an absorbance of about 0.1 at the excitation wavelength.

Transient Absorption (TA) Spectroscopy. TA measurements were performed with two pump−probe setups. The fs−ps TA setup used to record spectra up to 1.7 ns with an irf of ca. 150 fs (fwhm) has been described in detail elsewhere.[64,76] Excitation was performed using 400 nm pulses generated by frequency doubling part of the output of a standard 1 kHz Ti:sapphire amplified system, or with 600 nm pulses produced with a home-built noncollinear optical parametric amplifier. The intensity of the pump pulses on the sample was ca. 1 mJ/cm^2. The ns−μs TA setup, used to record spectra up to 5 μs with an irf of 370 ps (fwhm) is the same as that described in ref 77, except that excitation was performed using a passively Q-switched, frequency-doubled Nd:YAG laser (Teem Photonics, Powerchip PNG-M02010) producing pulses at 532 nm with 500 Hz repetition rate, 24 μJ energy per pulse, and 300 ps duration. The pump intensity on the sample was also around 1 mJ/cm^2. In both setups, probing was achieved using white light pulses generated by focusing 800 nm pulses in a CaF_2 plate and polarized at a magic angle relative to the pump pulses. The sample solutions were located in a 1 mm quartz cell and, unless specified, were continuously stirred by N_2 bubbling. Their absorbance at the excitation wavelength was around 0.1.

Quantum Chemical Calculations. Ground-state gas-phase geometry optimization of the dyads, with hydrogen instead of bromo substituents and methyl instead of octyl substituents on the imide N atoms was performed at the density functional level of theory (DFT) using the B3LYP functional and the 6-31G* basis set.[78] Electronic transitions were computed with time-dependent DFT (TD-DFT) using the same functional and basis set.[79] All calculations were performed using Gaussian 09.[80] Given the low barrier for rotation of the phenyl substituents of the porphyrins,[81] several geometries of similar energy but with different dihedral angles between the porphyrin and HNDI molecular planes were found. However, as the shape and relative energy of the frontier molecular orbitals were found to be qualitatively very similar in all the conformations investigated, these computational results can be reliably used to discuss the nature of the lowest electronic excited states.

RESULTS

Steady-State Spectroscopy. The electronic absorption spectra of the dyads in toluene are characterized by an intense band centered around 420 nm, that can be ascribed to the Soret or B band of the porphyrin, and by three weaker bands located at 517, 556, and 601 nm for both **1** and **2** (Figure 1). These bands are very similar to those observed with HNDI alone,[82] the only difference being a ~10 nm (310 cm^{-1}) blue shift and a narrowing that can be explained by the interaction with the porphyrin (Figure 1). HNDI also exhibits an absorption band in the 400−425 nm region that is, however, much too weak relative to the porphyrin B band to be visible in the dyad spectrum. Similarly, absorption due to the Q-bands of the porphyrins is not visible due to the overlap with the stronger HNDI bands except for **2**, for which the $Q_x(0,0)$ band of FbP

DOI: 10.1021/jp5108685
J. Phys. Chem. B 2015, 119, 7308−7320

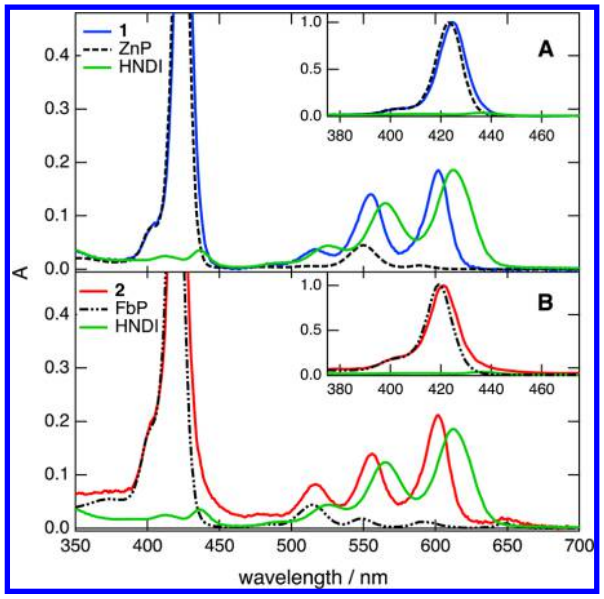

Figure 1. Electronic absorption spectra of the dyads (A) **1** and (B) **2** and of the individual constituents in toluene (the insets show the B band region).

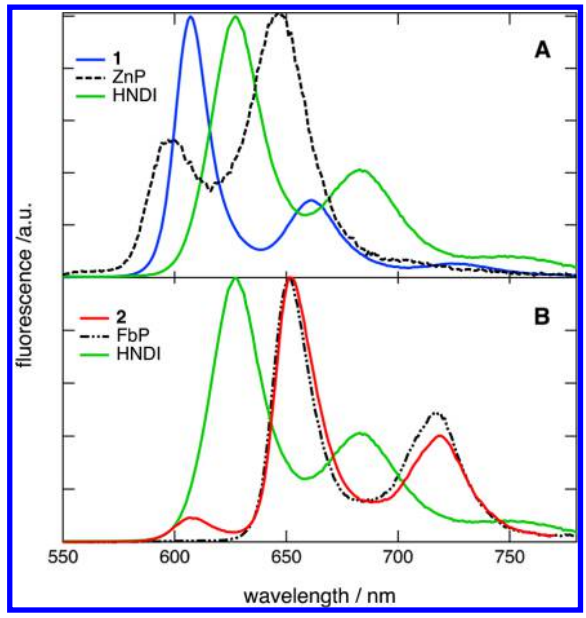

Figure 2. Fluorescence spectra of the dyads (A) **1** and (B) **2** and of the individual constituents in toluene.

can be observed at 650 nm (Figure 1B). No significant difference was observed in THF. Apart from some small spectral shifts, these spectra are essentially the composites of those of the porphyrins and HNDI and point to a weak coupling between the chromophores. Therefore, these absorption bands can be ascribed to transitions to locally excited states. In the following, we will call these states, ^1L_B, ^1L_Q, and ^1L_N for locally excited singlet B and Q porphyrin states and locally excited singlet NDI state, respectively.

TD-DFT calculations confirm that the first two electronic transitions with significant oscillator strength correspond to excitations from and to molecular orbitals localized on either the porphyrin or the HNDI units (Figure S1 of the Supporting Information).

Independent of the excitation wavelength, the emission spectrum of **1** in toluene consists of three bands with decreasing intensity and located at 607, 661, and 725 nm (Figure 2A). This spectrum is essentially a mirror image of absorption spectrum in the 500−600 nm region and can be attributed to the HNDI unit. This is confirmed by the fluorescence spectrum of HNDI that is very similar but red-shifted by ∼20 nm (520 cm^{-1}) and by the emission spectrum of ZnP that differs considerably with bands around 600 and 650 nm. Moreover, the fluorescence quantum yield of **1** was found to be 10 times as large as that of ZnP. The result points to an efficient EET from the ZnP to the HNDI unit (i.e. to a $^1L_Q \rightarrow {}^1L_N$ transition). In THF, the fluorescence of **1** is totally suppressed pointing to a fast nonradiative decay process of the excited state.

Contrary to **1**, dyad **2** fluoresces in both toluene and THF with a spectrum dominated by two bands at 650 and 718 nm, similar to that of FbP (Figure 2B). A smaller band at 607 nm, which can be attributed to HNDI, is also visible. The fluorescence quantum yield of **2** in toluene is 1.5 times larger than that of FbP and is reduced by a factor 2 when using THF as a solvent. These spectra point to EET in the opposite direction than in **1** (i.e., to a $^1L_N \rightarrow {}^1L_Q$ EET). The presence of a residual HNDI band, which is independent of the excitation wavelength, is a possible indication of an equilibrium between the ^1L_N and ^1L_Q states.

Time-Resolved Fluorescence. The fluorescence dynamics of **1** in toluene measured by TCSPC at several wavelengths between 600 and 720 nm upon $^1L_B \leftarrow S_0$ excitation of the ZnP unit could be well-reproduced using a single exponential decay with a 2.8 ns lifetime (Table 1). This time constant coincides well with that of 2.7 ns measured with HNDI in toluene, confirming the occurrence of EET from ZnP to HNDI.

Table 1. Time Constants Obtained from the Analysis of the Fluorescence Dynamics Measured by FU (τ_{1-3}, Limit of Error: ±10%) and TCSPC (τ_4, Limit of Error: ±5%)[a]

dyad	solvent	λ (nm)	τ_1 (ps)	τ_2 (ps)	τ_3 (ps)	τ_4 (ns)
1	toluene	610−660	0.48[c]	13[d]		2.8[b]
1	toluene	430−450	0.31[b]			
1	THF	610−660	0.30[c]	18[b]		
1	THF	430−450	0.32[b]			
2	toluene	610	≤irf	2.4	15	9.2[b,e]
2	toluene	650, 715	1.8	25		9.2[b]
2	THF	610	≤irf	1.6	11	4.8[b]
2	THF	650, 715	1.8	20		4.9[b]

[a]Unless specified, the time constants correspond to decay times. [b]These values are assigned to excited-state lifetimes. [c]Rise time. [d]Rise time at 610 nm. [e]Weak 2.45 ns component also present.

Ultrafast fluorescence measured by FU reveals more complex dynamics (Figure 3 and Table 1). Time profiles at 610, 650, and 660 nm could be analyzed globally using the sum of three exponential functions with 480 fs, 13 ps, and 2.8 ns time constants. The latter, taken from the TCSPC results, was kept constant during the fit. At all three wavelengths, the amplitude of the 480 fs component is negative pointing to an increase of the overall fluorescence intensity. In principle, this time constant could be due to two processes, depending on whether emission arises from the ZnP or the HNDI unit: (i) internal conversion from the ^1L_B to the ^1L_Q states of ZnP or (ii) $^1L_Q \rightarrow {}^1L_N$ EET. The 2.8 ns lifetime indicates that emission should

DOI: 10.1021/jp5108685
J. Phys. Chem. B 2015, 119, 7308−7320

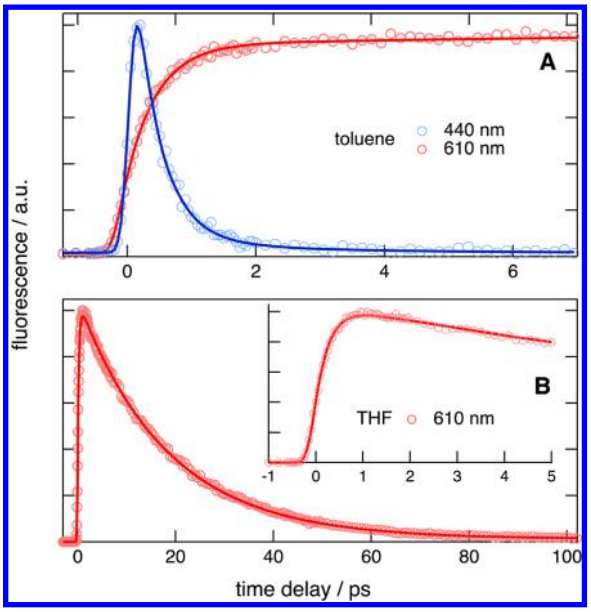

Figure 3. Fluorescence dynamics at 440 and 610 nm measured with dyad **1** in (A) toluene and (B) THF and best multiexponential fits.

arise from HNDI. Furthermore, the extinction coefficient of the HNDI band and thus the radiative rate constant of the $^1L_N \rightarrow S_0$ emission is substantially larger than that of the ZnP Q-band (Figure 1A). Due to this, the contribution of ZnP emission to the FU signal intensity should be much weaker than that of HNDI. As a consequence, the 480 fs time component most probably reflects the population of the ^1L_N state by EET.

The amplitude associated with the 13 ps component is relatively small (<0.2), and its sign changes from negative at 610 nm to positive at longer wavelengths. Given that a large fraction of the excitation energy is converted into vibrational energy, this component most likely arises from vibrational cooling.[83]

FU measurements were also performed in the 430−450 nm region where B emission from the ZnP unit ($^1L_B \rightarrow S_0$) is expected. As shown in Figure 3A, the fluorescence decay is extremely fast, close to the irf, and can be reproduced using a single exponential function with a 310 ± 30 fs time constant. This is shorter than the rise time of the fluorescence above 600 nm. This time constant can thus be assigned to $^1L_B \rightarrow {}^1L_Q$ internal conversion. This process is much faster in **1** than in ZnP alone, where it occurs with a 1.4 ps time constant in benzene.[84] Such acceleration can be explained by structural distortions of ZnP brought about by substitution of this highly symmetric molecule and has been previously observed in ZnP based multichromophoric systems.[85−87]

As anticipated from the absence of steady-state emission, the fluorescence decay of **1** in THF above 600 nm was too fast to be resolved by TCSPC. FU time profiles between 610 and 660 nm could be reproduced with a biexponential function, with a 300 fs rise time and a 18 ps decay time (Figure 3B and Table 1).

The fluorescence dynamics in the 440−460 nm region is characterized by a 320 ± 30 fs decay time, very close to the 300 fs rise time. This rise time could be due to either $^1L_B \rightarrow {}^1L_Q$ internal conversion or ZnP to HNDI EET. This point is discussed in more depth in Transient Absorption.

The fluorescence decay of dyad **2** in toluene at 650 and 715 nm measured by TCSPC is exponential with a 9.2 ns lifetime, slightly shorter than that of 11 ns reported for FbP in the same solvent.[88] It can thus be attributed to $^1L_Q \rightarrow S_0$ emission from the porphyrin moiety. The fluorescence decay of the 610 nm band, which arises from the HNDI unit, is also dominated by a 9.2 ns lifetime but an additional 2.45 ns component with weak amplitude is also observed. The presence of a common decay time of 9.2 ns for both $^1L_Q \rightarrow S_0$ and $^1L_N \rightarrow S_0$ emissions points to an equilibrium between the two locally excited states, largely in favor of that localized on the porphyrin unit. The origin of the 2.45 ns component is unclear, but its similarity with the decay time of HNDI suggest that it could arise from traces of unreacted compound **3**.

The early 650 nm fluorescence of **2** in toluene measured by FU is very similar to that reported earlier with FbP alone and exhibits decay components with 2 and ∼20 ps, additionally to the nanosecond decay, that can be ascribed to various stages of vibrational relaxation.[89] Contrary to ZnP, the B state of FbP is extremely short-lived, <50 fs, and thus cannot be observed.[89] On the other hand, the fluorescence at 610 nm looses about 99% of its initial intensity within ∼30 ps, with 0.2, 2.4, and ∼15 ps time constants (Table 1). The residual intensity has too small an amplitude to allow a relevant time constant to be extracted. However, this slow component corresponds to the emission measured by TCSPC and dominated by a 9.2 ns lifetime. A definite assignment of the short time constants is difficult. Excitation at 420 nm results mostly in the population of the B state of FbP. As rather similar decay dynamics have been reported with FbP at 613 nm,[89] these short time constants are attributed to vibrational relaxation of the FbP unit.

In THF, the fluorescence dynamics of **2** measured by TCSPC between 610 and 720 nm is faster than in toluene and is characterized by a 4.9 ns decay. Conversely, the early dynamics measured by FU is essentially the same as in toluene (Table 1).

Transient Absorption. TA measurements between 0 and 1.7 ns were performed upon 400 and 600 nm excitation, resulting to a larger extent in the population of the ^1L_B and ^1L_N states, respectively. Figure 4A illustrates selected TA spectra recorded during the first 15 ps after 400 nm excitation of **1** in toluene. They are characterized by negative bands around 425, 557, and 605 nm, that can be assigned to the bleach of the $^1L_B \leftarrow S_0$ and $^1L_N \leftarrow S_0$ transitions and by broader and less intense positive bands. During this time window, the $^1L_B \leftarrow S_0$ bleach decreases, whereas the $^1L_N \leftarrow S_0$ increases. Afterward, the overall spectral shape does not change significantly, but the amplitude decreases continuously on a timescale that exceeds the time window of the experiment. The temporal evolution of the TA spectra was analyzed globally, using the sum of three exponential functions with 0.5 ps, 11 ps, and >2 ns time constants and the decay associated difference spectra (DADS) shown in Figure 4B. The 0.5 ps DADS points to a decrease of the ZnP $^1L_B \leftarrow S_0$ bleach and an associated increase of the HNDI $^1L_N \leftarrow S_0$ bleach. This is a univocal evidence of the ZnP → HNDI EET that was already anticipated from the stationary and time-resolved fluorescence measurements. The 0.5 ps value agrees with that obtained from the analysis of the FU data in the 610−660 nm region.

The 11 ps DADS also points to an increase of the $^1L_N \leftarrow S_0$ bleach. However, this DADS exhibits a dispersive-like band in the 400−450 nm region that is characteristic of a vibrationally hot ground state, with a positive band on the red side of the bleach.[90,91] As a consequence, this 11 ps component could reflect two processes: (i) slower EET stages and (ii) the

DOI: 10.1021/jp5108685
J. Phys. Chem. B 2015, 119, 7308−7320

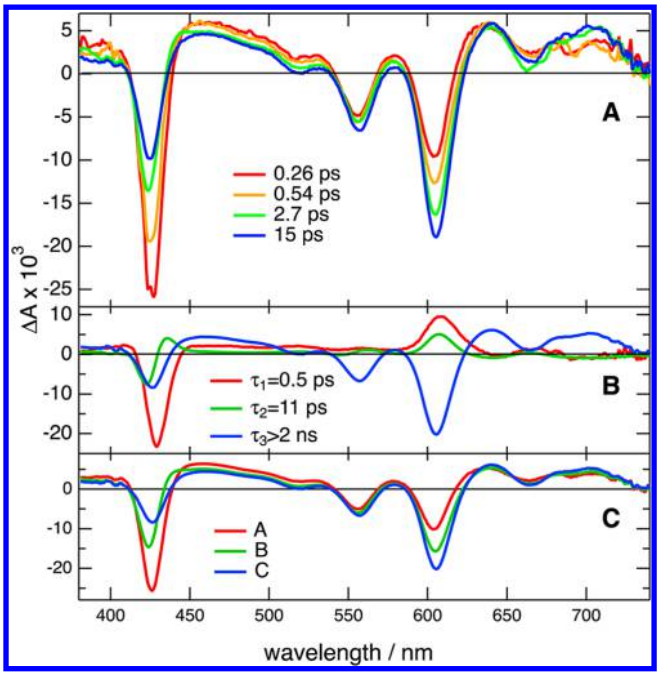

Figure 4. (A) Transient absorption spectra measured at different time delays after 400 nm excitation of **1** in toluene, (B) decay-associated, and (C) species-associated difference absorption spectra obtained from (B) global multiexponential analysis and (C) target analysis assuming an A → B → C → D scheme.

vibrational cooling of the ZnP moiety in the electronic ground state after the transfer of its electronic energy to the HNDI unit. As $^1L_B \rightarrow {}^1L_Q$ internal conversion is very fast, EET should take place from the ZnP unit in the ^1L_Q state. This state is initially populated with a very large vibrational energy, which should mainly remain in the ZnP unit after the transfer of the electronic energy.

Global target analysis assuming a scheme with three successive exponential steps, A → B → C → D, was also performed. This approach yielded the same time constants, as expected,[92] and the species-associated difference spectra (SADS) for A, B, and C shown in Figure 4C. The presence of the HNDI $^1L_N \leftarrow S_0$ bleach in the SADS of A is probably due to the fact that EET is ultrafast, close to the irf, and that its dynamics might be non exponential.[93] Despite this, the SADS qualitatively agree with a scheme where A is the dyad in the ^1L_Q state, B the dyad in the ^1L_N state with the vibrationally hot ZnP unit, and C the dyad in the ^1L_N state after vibrational relaxation.

The presence of a residual $^1L_B \leftarrow S_0$ bleach in the SADS of B and C could have at least two origins: (i) the delocalization of the excitation over the whole dyad, and (ii) back EET from the HNDI to the ZnP units (i.e., the existence of an equilibrium between the ^1L_Q and ^1L_N states).

The TA spectra recorded upon 600 nm excitation also exhibit the negative bands due to the bleach of the $^1L_B \leftarrow S_0$ and $^1L_N \leftarrow S_0$ absorption (Figure S2A of the Supporting Information). However, their relative intensity in the early spectra differs from that observed upon excitation at 400 nm. Indeed, the $^1L_B \leftarrow S_0$ bleach upon 600 nm excitation is substantially smaller and is similar to that observed upon 400 nm excitation but after about 20 ps, once EET to the HNDI unit has taken place.

The temporal evolution of the TA spectra could be reproduced using the sum of two exponential functions and a A → B → C scheme with ∼1.4 ps and >2 ns time constants and the DADS and SADS shown in Figure S2B–S2C of the Supporting Information. The amplitude of the shorter time constant is too small to enable a precise assignment. However, the D(S)ADS points to a decrease of the TA amplitude over the whole spectrum but to a larger extent for the HNDI features. This time constant could thus reflect some back EET from HNDI to ZnP and the establishment of an equilibrium between the ^1L_Q and ^1L_N states. This point will be discussed further below. On the other hand, the >2 ns DADS is very similar to that obtained from the 400 nm excitation data (Figure 4B).

The slower stages of the excited-state dynamics of **1** in toluene were monitored using the ns–μs TA setup with 532

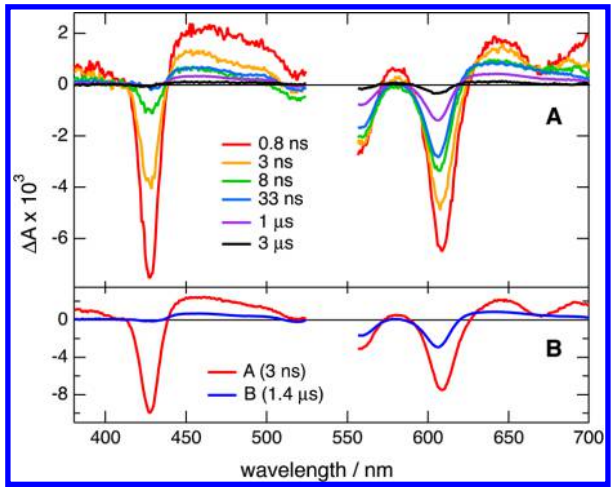

Figure 5. (A) Transient absorption spectra measured at different time delay after 532 nm excitation of **1** in toluene; (B) species-associated difference absorption spectra obtained from global target analysis assuming an A → B → C scheme.

nm pump pulses (Figure 5A). The TA spectra show that the $^1L_B \leftarrow S_0$ bleach decays entirely to zero within a few tens of nanoseconds. During this time interval, the $^1L_N \leftarrow S_0$ bleach decreases by a factor of about 2 only, the full decay taking place on the microsecond timescale. In the presence of air, this decay is accelerated by a factor of about 3. Global analysis could be performed using an A → B → C scheme with 3 ns and 1.4 μs time constants and the SADS shown in Figure 5B. The A → B step corresponds to a transition to a long-lived excited state localized on the HNDI unit, that given the sensitivity of its lifetime to oxygen, can be attributed to the locally excited triplet state, ^3L_N. From the amplitude of the $^1L_N \leftarrow S_0$ bleach in the A and B SADS, the triplet yield of **1** can be estimated to be around 0.3.

The TA spectra of **1** in THF exhibit the same bands as in toluene, but the overall dynamics is much faster (Figure 6A). Upon 400 nm excitation, the initial increase of the $^1L_N \leftarrow S_0$ bleach which is characteristic of ZnP → HNDI EET can be observed. However, it is followed by a decay of all spectral features on a ∼50 ps timescale. The TA spectra also feature a small and narrow positive band at 410 nm that is absent in toluene. This band reaches its maximum intensity at about 30 ps and then decays similarly to the others. The position and shape of this band are very similar to those observed with other

DOI: 10.1021/jp5108685
J. Phys. Chem. B 2015, 119, 7308–7320

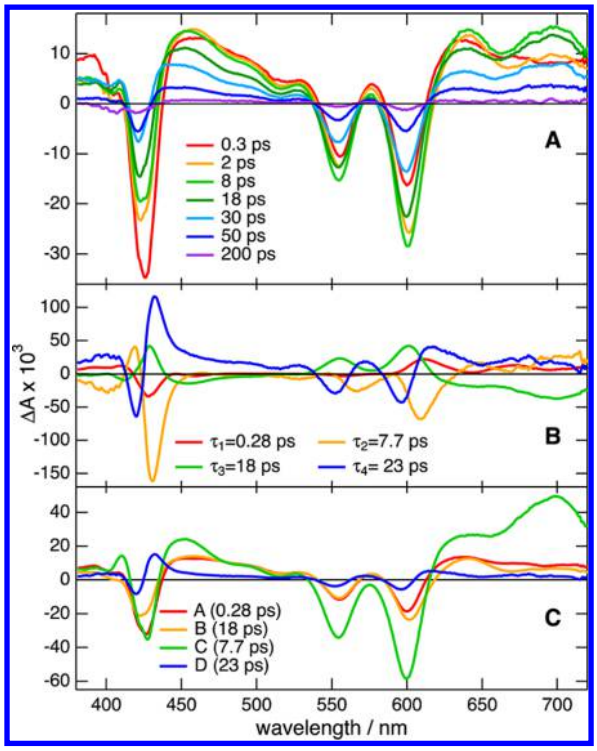

Figure 6. (A) Transient absorption spectra measured at different time delays after 400 nm excitation of **1** in THF; (B) decay-associated and (C) species-associated difference absorption spectra obtained from (B) global multiexponential analysis and (C) target analysis assuming an A → B → C → D → E scheme.

ZnP-based electron donor−acceptor dyads and attributed to the ZnP radical cation, $ZnP^{\cdot+}$.[87,94,95]

All these bands are also present in the TA spectra recorded upon 600 nm excitation (Figure S3A of the Supporting Information). However, several differences in the early dynamics are observed: (i) the $^1L_N \leftarrow S_0$ bleach does not exhibit any initial increase, and (ii) the $^1L_B \leftarrow S_0$ bleach increases up to ∼7 ps before decaying as with excitation at 400 nm.

Multiexponential global analysis of the TA spectra recorded upon 400 nm excitation required the sum of four exponential functions with the time constants listed in Table 2 and the DADS shown in Figure 6B. From the DADS, the shortest time constant can be ascribed to the ZnP → HNDI EET and to the establishment of an equilibrium between the ^1L_Q and ^1L_N states. The assignment of the other time constants from their DADS is more difficult. According to the FU measurements, the 18 ps time constant can be assigned to the nonradiative decay of the fluorescent state of **1**, that is most probably a charge separation (CS) process considering the lifetime shortening by going from a nonpolar to a polar solvent and the presence of the $ZnP^{\cdot+}$ band. However, the 18 ps DADS points to a decay of the $ZnP^{\cdot+}$ band and of both $^1L_B \leftarrow S_0$ and $^1L_N \leftarrow S_0$ bleaches. Such apparent contradiction could be explained by an inverted kinetics, namely a CS process that is slower than the ensuing charge recombination (CR) to the neutral ground state.[96] To test this hypothesis, global target analysis assuming a scheme with four successive exponential steps, A → B → C → D → E, with the B → C step fixed at 18 ps was performed and yielded the species-associated difference absorption spectra (SADS) shown in Figure 6C. From these spectra, species A and B can be attributed to dyad **1** predominantly in the ^1L_Q and ^1L_N states, respectively. The SADS of C contains the $ZnP^{\cdot+}$ band, negative bands due to the bleach of both ZnP and HNDI units and can thus be ascribed to a charge-separated state (CSS). The other positive TA bands at 450 and 700 nm could possibly be due to the HNDI anion, $HNDI^{\cdot-}$.[41,97] As a consequence, the 18 ps time constant can be attributed to CS, in agreement with the FU measurements. The 7.7 ps decay of the CSS results in a "species" with a spectrum exhibiting dispersive bands (i.e., with a positive feature on the red side of a bleach, which is typical of a vibrational hot ground state). Thus, the 7.7 ps time constant corresponds to the CR time constant, whereas the 23 ps lifetime can be assigned to the vibrational cooling of the ground state.

Target analysis of TA spectra upon 600 nm excitation with a B → C → D → E scheme did not allow the early dynamics to be properly reproduced and, thus, a scheme with five successive exponential steps had to be used as well, with the time constants listed in Table 2 and the SADS shown in Figure S3C of the Supporting Information. The SADS of B, C, D, and E and the associated time constants are similar to those obtained from the 400 nm excitation data and can thus be interpreted likewise. On the other hand, the SADS of A differs from that of B by a smaller $^1L_B \leftarrow S_0$ bleach and a larger $^1L_N \leftarrow S_0$ bleach. Thus, the A → B step could correspond to the establishment of the above-mentioned equilibrium between the ^1L_Q and ^1L_N states.

The TA spectra recorded upon excitation at 400 and 600 nm of **2** in toluene and THF are shown in Figure 7 (panels A and B) and Figure S4 (panels A and B) of the Supporting Information. Independent of the excitation wavelength and solvent, these spectra are dominated by negative bands around 420 nm and in the 520−620 nm region, that can be ascribed to the bleach of the $^1L_B \leftarrow S_0$, $^1L_Q \leftarrow S_0$, and $^1L_N \leftarrow S_0$ absorption,

Table 2. Time Constants Obtained from the Analysis of the fs−ps (τ_{1-4}) and ps−μs ($\tau_{5,6}$) Transient Absorption (Limit of Error ± 10% Unless Specified)

dyad	solvent	λ (nm)	τ_1 (ps)	τ_2 (ps)	τ_3 (ps)	τ_4 (ps)	τ_5 (ns)	τ_6 (μs)
1	toluene	400	0.5	11			>2	
1	toluene	600/532	∼1.4[a]				3.0	1.4
1	THF	400	0.28	7.7	18	23		
1	THF	600	0.63	7.7	18	23		
2	toluene	400	∼1.5[a]	95				
2	toluene	600/532	2.7	97			10	1.1
2	THF	400	∼4[a]					
2	THF	600/532	2.7				5	1.0

[a]Only approximate value, due to a very small amplitude.

DOI: 10.1021/jp5108685
J. Phys. Chem. B 2015, 119, 7308−7320

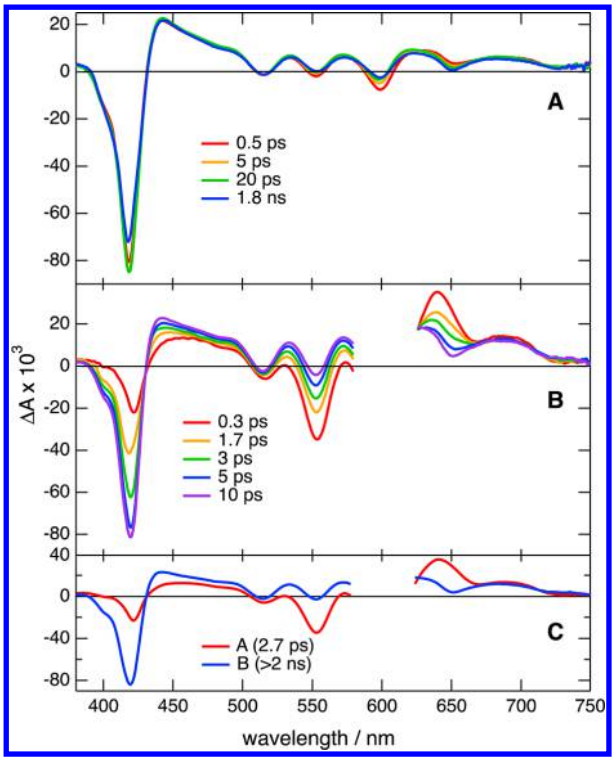

Figure 7. Transient absorption spectra measured at different time delays after (A) 400 and (B) 600 nm excitation of **2** in (A) THF and species-associated difference absorption spectra obtained from global target analysis of the 600 nm data assuming (C) an A → B → C scheme.

respectively. Substantial dependence of the relative intensity and temporal evolution of these bands on the excitation wavelength can be observed. At 400 nm, which mostly corresponds to the local excitation of FbP, the $^1L_N \leftarrow S_0$ bleach is hardly visible and decreases within a few picoseconds, whereas the intense $^1L_B \leftarrow S_0$ bleach increases slightly. Afterward, the TA spectra remain essentially constant in THF (Figure 7A), whereas in toluene, small changes especially around 440 nm can be observed on a 100 ps timescale (Figure S4A of the Supporting Information)

Upon 600 nm excitation, the initial $^1L_N \leftarrow S_0$ bleach is more intense than the $^1L_B \leftarrow S_0$ bleach (Figure 7B and Figure S4B of the Supporting Information). During the first 10 ps, the former decreases almost entirely, whereas the latter increases by a factor of ~4. From about 10 ps onward, the TA spectra and their temporal evolution are essentially the same as upon 400 nm excitation.

Global analysis of the data in toluene could be performed successfully with the sum of three exponential functions with ~2 ps, 95 ps, and >2 ns time constants independently of the excitation wavelength (Table 2). In THF, two exponential functions with ~2 ps and >2 ns time constants were sufficient, and a target analysis assuming an A → B→ C scheme gave the SADS shown in Figure 7C. In both solvents, the amplitude of the fastest component is much larger for 600 nm than 400 nm excitation and thus the time constant obtained from the 600 nm data, namely 2.7 ps, is more reliable. From the SADS that point to a decrease of the $^1L_N \leftarrow S_0$ bleach and an increase of the $^1L_B \leftarrow S_0$ bleach when going from A to B, the A → B step can be ascribed to EET from the HNDI to the FbP unit. Not surprisingly, this process is hardly visible upon excitation at 400 nm. The >2 ns component agrees with the nanosecond fluorescence lifetime (Table 1). The assignment of the 95 ps time constant found only in toluene is more difficult as its amplitude is relatively small (Figure S4C of the Supporting Information). We tentatively attribute it to the decay of excited aggregates. Indeed, contrary to **1**, the absorption bands of **2** in toluene at the concentration used for the TA measurements are markedly broader than at lower concentrations or in THF, where this 95 ps component is absent. Such broadening and accelerated excited-state decay have already been reported for another FbP-based dyad.[82]

The TA spectra measured at longer time delays upon 532 nm, $^1L_N \leftarrow S_0$, excitation of **2** in toluene are illustrated in Figure 8 (panels A and B). Between 0.2 to about 50 ns, they show the

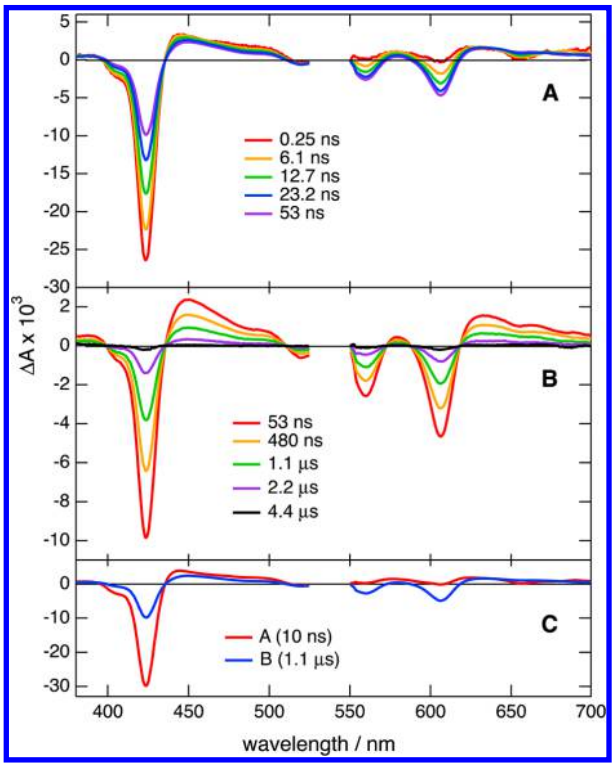

Figure 8. (A and B) Transient absorption spectra measured at different time delays after 532 nm excitation of **2** in toluene and species-associated difference absorption spectra obtained from global target analysis (C) assuming an A → B → C scheme.

opposite behavior than during the first 10 ps (Figure 7B) (i.e., a decrease of the $^1L_B \leftarrow S_0$ bleach and an increase of the $^1L_N \leftarrow S_0$ bleach), pointing to a transfer of energy from the FbP to the NDI moiety. During this process, the $^1L_B \leftarrow S_0$ bleach decreases to only about 1/3 of its initial value. After about 50 ns, the overall spectral shape remains constant and the intensity decays to zero on the microsecond timescale (Figure 8B). Global analysis indicates that the time constants of these two processes amount to 10 ns and 1.1 μs. In the presence of air, the long time constant shortens to 415 ns. As a consequence, the longer-lived transient can be ascribed to a triplet excited state. Its SADS exhibits both the FbP and the HNDI bleach bands, suggesting an equilibrium between the triplet excited states localized on the HNDI and FbP moieties, namely the ^3L_N and ^3L_Q states (Figure 8C).

The 10 ns time constant is in good agreement with the fluorescence lifetime and can thus be ascribed to the decay of

DOI: 10.1021/jp5108685
J. Phys. Chem. B 2015, 119, 7308−7320

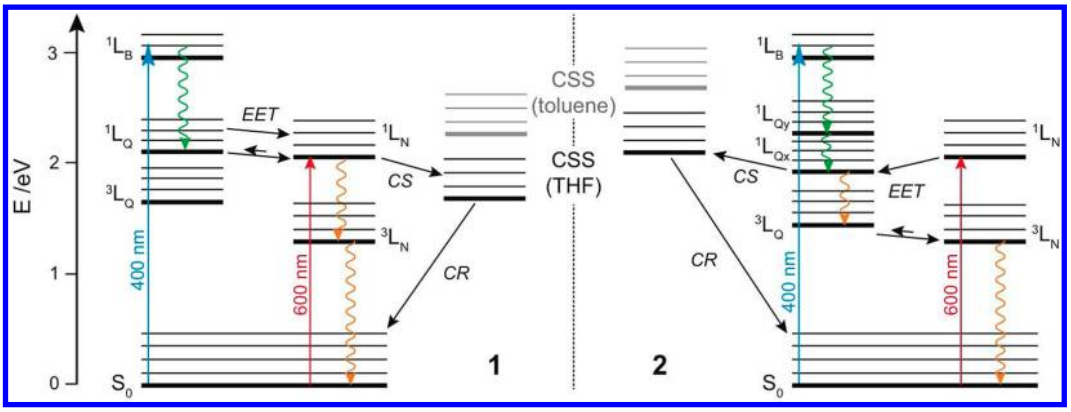

Figure 9. Energy level scheme of dyads **1** (left) and **2** (right) with the dominant processes (green wavy arrows: internal conversion; orange wavy arrows: intersystem crossing).

the ^1L_Q state by both fluorescence and intersystem-crossing (ISC) to the ^3L_Q state. Being spin-allowed, the FbP → HNDI triplet energy transfer and the reverse processes can be expected to be much faster than the ^1L_Q → ^3L_Q ISC. If this were not the case, TA spectra exhibiting only the ^3L_Q state should be observed.

By going from toluene to THF, only two significant differences in the slow TA dynamics of **2** can be observed (Figure S5 of the Supporting Information). The first is the shortening of the nanosecond time constant from 10 to 5 ns, also observed by fluorescence. The second is the amplitude of the SADS of the long-lived triplet state of **2**, which is about twice as small as in toluene. These differences point to the opening of a new nonradiative decay pathway of the ^1L_Q state in THF that shortens its lifetime by a factor of two and competes with ISC and the ensuing triplet energy transfer. As will be discussed in more detail in the next section, this channel is likely a CS process followed by a much faster recombination to the neutral ground state.

DISCUSSION

Figure 9 shows the energy-level scheme of both dyads, with the energy of the local singlet excited states determined from the stationary electronic spectra and that of the local triplet state of the porphyrin units assumed to be the same as that of the individual porphyrins.[98] On the other hand, the energy of the ^3L_N state is not known and has been estimated from the direction of the triplet energy transfer (TET) processes found here and discussed in more detail below. Finally, the energy of the CSS (E_{CSS} = 1.84 eV for **1** and 2.1 eV for **2**) has been estimated using the Weller equation[99] as described in detail in the Supporting Information. In toluene, the CSS is destabilized by about 0.6 eV because of the reduced solvation energy. The rate constants of the most relevant processes are summarized in Table 3.

These schemes reveal that the relative energies of the local singlet excited states, ^1L_Q and ^1L_N, are inverted when going from **1** to **2** (i.e., ^1L_Q is above ^1L_N with ZnP but below ^1L_N with FbP). This is fully consistent with the stationary fluorescence spectra of the dyads as well as with the EET processes observed during the first few picoseconds after excitation: ^1L_Q → ^1L_N energy transfer takes place with **1**, whereas ^1L_N → ^1L_Q transfer is occurring in **2**. The TA data of **1** indicate that this EET is not fully irreversible and that both ^1L_N and ^1L_Q states are in equilibrium. From the intensity of the ^1L_B ← S_0 bleach bands in the SADS of A and C (Figure 4C), about one-fifth of the

Table 3. Time Constants of the Most Relevant Processes in Dyads 1 and 2[a]

dyad	process	τ	dyad	process	τ
1	EET ^1L_Q → ^1L_N	0.5 ps	**2**	EET ^1L_N → ^1L_Q	2.7 ps
1	CS ^1L_N → CSS	18 ps	**2**	CS ^1L_Q → CSS	10 ns
1	CR CSS → S_0	7.7 ps	**2**	CR CSS → S_0	≪ 10 ns
1	ISC ^1L_N → ^3L_N	9.3 ns[b]	**2**	ISC ^1L_Q → ^3L_Q	14 ns[c]
1	ISC ^3L_N → S_0	1.4 μs	**2**	EET ^3L_Q → ^3L_N	≪10 ns
			2	ISC ^3L_N → S_0	1 μs

[a]Apart from the charge separation and recombination processes that occur only in THF, the other processes show little solvent dependence. [b]Using a triplet quantum yield of 0.3. [c]Using a triplet quantum yield of 0.7.[98]

excited dyad population remains in the ^1L_Q state, pointing to an equilibrium constant of ca. 4. Such an equilibrium cannot be evidenced from the TA data with **2**, as no residual ^1L_N ← S_0 bleach can be clearly distinguished. However, the presence of a small HNDI contribution in the stationary spectrum of **2** in toluene (Figure 2B) with the same fluorescence lifetime as FbP points to an equilibrium, but strongly in favor of the ^1L_Q state. This is consistent with the energy gap between these two states, which is about three times as large for **2** as for **1**.

EET between two weakly coupled chromophores, as it is the case here, can occur through both the Coulomb and the exchange interactions (i.e., the Förster (FRET) and the Dexter mechanisms).[100,101] The overall rate constant can be expressed as the sum of the rate constants associated with each process:[102]

$$k_{EET} = k_C + k_e = \frac{2\pi}{\hbar}(V_C^2 + V_e^2)\Theta \quad (1)$$

where V_C and V_e are the Coulomb and exchange interaction energies, respectively, and Θ is the spectral overlap integral, obtained from the area-normalized emission and absorption bands of the energy donor (D) and acceptor (A), respectively. In accordance with this equation, the relative magnitude of the EET rate constants found with **1** and **2** can be estimated from that of Θ. As the electronic absorption and emission of the HNDI are altered in the dyads, the calculation of Θ was performed using those of HNDI shifted to shorter wavelengths to match the dyads spectra. The resulting Θ values, listed in Table 4, indicate that energy transfer from ZnP to HNDI (^1L_Q → ^1L_N) is indeed more favorable than that in the opposite direction (^1L_N → ^1L_Q). They also confirm the results found

DOI: 10.1021/jp5108685
J. Phys. Chem. B 2015, 119, 7308−7320

Table 4. Rate Constants for EET from D to A via the Förster Mechanism Calculated Using eq 1 and Associated Parameters

D	A	V_C (cm^{-1})	$\Theta \times 10^5$ (cm)	$1/k_C$ (ps)
ZnP	HNDI	42	16.3	2.9
HNDI	ZnP	42	2.2	22
FbP	HNDI	29	0.3	330
HNDI	FbP	29	26	3.8

with **2**, that energy transfer occurs from HNDI to FbP ($^1L_N \rightarrow {}^1L_Q$) and that the reverse process is much slower.

Knowledge of the interaction energies, V_C and V_e, is necessary to determine which of the Förster or Dexter mechanism dominates. Whereas V_e depends on the overlap integral of the molecular orbitals of the "exchanged" electrons, V_C can be estimated relatively easily according to Förster theory from the interaction between the dipole moments for the D* → D and A* ← A transitions, μ_D and μ_A at a distance d_{DA}:

$$V_C = \frac{\mu_D \mu_D f_L^2}{4\pi\varepsilon_0 \varepsilon_{op} d_{DA}^3}\kappa \qquad (2)$$

where $\varepsilon_{op} \simeq n^2$ is the dielectric constant at optical frequencies, n being the refractive index of the solvent, $f_L = (\varepsilon_{op} + 2)/3$ is the Lorentz local field correction factor and κ the orientational factor (eq S3 of the Supporting Information). The details of the calculations of V_C are given in the Supporting Information and the resulting Coulomb interaction energies and rate constant, k_C, are listed in Table 4.

This table reveals a very good agreement between the measured and calculated time constants with **2** (i.e., 2.7 vs 3.9 ps). The situation is different with dyad **1**, for which the calculated time constant is similar to that for **2** but the measured one is about 6 times smaller. Such a faster EET with **1** is surprising considering the similarity in size of the dipole moments for the Q transition in ZnP and FbP and the similar Θ values. A contribution of the Dexter mechanism cannot be ruled out, but, given that both dyads have the same peptide linker, major differences in V_e is not expected. To account for the faster energy transfer in **1**, the V_e should amount to about 90 cm^{-1} (i.e., twice as large as V_C). Furthermore, as shown in Figure S1 of the Supporting Information, the molecular orbitals of the exchanged electrons remain localized on a single chromophoric unit and point to a rather modest V_e.

The above calculations assume that EET occurs from a thermally equilibrated excited state. Such assumption is most probably not correct for dyad **1** upon $^1L_B \leftarrow S_0$ excitation. ZnP not only emits from the ^1L_B state but also exhibits significant fluorescence from the vibrationally hot ^1L_Q state, populated upon internal conversion from ^1L_B. The hot Q fluorescence of ZnP differs from that of the equilibrated fluorescence by a much more intense vibronic band around 555 nm and a 3−5 ps lifetime.[84] Consequently, the spectral overlap integral for ZnP → HNDI EET is substantially larger when the Q state is vibrationally hot. Additionally, because of vibronic coupling with the upper ^1L_B state, the transition dipole moment for hot emission can be expected to be larger than that for the equilibrated emission.[103] These two factors (i.e., increase of Θ and V_C) are probably sufficient to account for the subpicosecond EET in **1**. This explanation is fully supported by the TA data upon excitation at 400 nm (Figure 4) that shows, that, after EET, the ZnP moiety is vibrationally hot. Even if EET takes place from a vibrationally excited state, only the vibrational energy associated with the vibronic transition is transferred to the acceptor, and the energy distributed in the other, Franck−Condon inactive, modes remains on the donor.

In principle, such a nonequilibrium process could also be predicted in **2** for the energy transfer from FbP to HNDI. However, as Q_y emission of FbP upon $^1L_B \leftarrow S_0$ excitation has been shown to be much shorter-lived, with a subpicosecond average lifetime,[89] such a process should not be very significant, especially considering the main EET in **2** is that from HNDI to FbP.

The TA spectra measured at long time delays with **2** (Figure 8) shows that after the ultrafast and quasi-irreversible $^1L_N \rightarrow {}^1L_Q$ EET, triplet energy transfer (TET) from the FbP to the HNDI unit (i.e., $^3L_Q \rightarrow {}^3L_N$) is taking place. This process occurs after the population of the ^3L_Q state, that is characterized by a 10 ns time constant. As this ^3L_Q state cannot be observed in the TA spectra, one can conclude that $^3L_Q \rightarrow {}^3L_N$ TET is significantly faster that ISC. Unfortunately, more quantitative dynamic information on this process is not accessible. The presence of a residual $^1L_B \leftarrow S_0$ bleach indicates that the reverse TET is also operative and, thus, that the ^3L_N and ^3L_Q are in equilibrium with a constant of ca. 2 in favor of ^3L_N. As a consequence, the ^3L_N state can be estimated to be just below ^3L_Q (i.e., around 1.4 eV). This is about 0.2 eV below the ^3L_Q state of **1** and explains why $^3L_N \rightarrow {}^3L_Q$ TET is not observed with this dyad.

TET occurs via the exchange mechanism, and its rate constant can be discussed in terms of eq 1 with $V_C \sim 0$.[104] However, determination of Θ requires knowledge of the phosphorescence and triplet absorption spectra of the energy donor and acceptor, which are not easily accessible.

The energy level schemes in Figure 9 reveal the presence of a CSS in **1** below the ^1L_Q and ^1L_N states in THF. For **2**, this state should be slightly above the ^1L_Q state. According to the redox potential of the constituents, and the TA data of **1**, the CSS consists of the oxidized porphyrin and the reduced HNDI. Such a state is also predicted by the TD-DFT calculations, which point to a transition with negligibly small oscillator strength corresponding to a one-electron HOMO−LUMO excitation, with the HOMO and LUMO entirely localized on the porphyrin and HNDI units, respectively (Figure S1 of the Supporting Information). Thus, CS from the ^1L_N state of **1** is a hole transfer, whereas CS from the ^1L_Q state in **2** is an electron transfer.

The driving force for CS, $-\Delta G_{CS}$, can be estimated to be around 0.2 and −0.2 eV for **1** and **2**, respectively. As the ^1L_Q and ^1L_N states of **1** are in equilibrium, ΔG_{CS} depends slightly on which of these states CS occurs from. Both the 18 ps and ∼10 ns CS time constants for **1** and **2** agree well with their respective driving force. CS in **1** is slower than in other ZnP/NDI-based arrays for which time contants of 1 and 5 ps were reported in THF.[67,87] In all these cases, ΔG_{CS} is of the same order of magnitude but the distance between the donor and acceptor varies (i.e., around 11.5 and 12.5 Å) because of different linkers,[67,87] versus ca. 14 Å in **1**. A logarithmic plot of the three CS rate constants versus the distance points to a reasonably linear dependence (r = 0.98, Figure S6 of the Supporting Information). Although this approach is very crude given the small number of points, it indicates that the larger donor−acceptor distance in **1** can account for the slower CS.

CR in **1**, with a 7.7 ps time constant, is not much slower than those found in the above-mentioned ZnP/NDI-based arrays (5

DOI: 10.1021/jp5108685
J. Phys. Chem. B 2015, 119, 7308−7320

and 3.2 ps, respectively).[67,87] In this case, however, the CR driving force is not the same for all three systems and varies between 1.3 and 1.8 eV. These values indicate that CR should be close to barrierless or in the onset of the inverted regime.

As the CR driving force in **2** should be significantly larger (i.e., around 2.1 eV), this process can be expected to be substantially slower but still much faster than CS. For this reason, the CS state of **2** cannot be observed in the TA experiments.

CONCLUDING REMARKS

The two porphyrin-naphthalenediimide dyads investigated here exhibit a very rich photophysics. This is due to the fact that both chromophores have electronic excited states of similar energies and to the nature of the bridge. A short or a conjugated bridge would increase the coupling and, given the closeness of the energy levels, favor strong excitonic interaction and thus a delocalization of the electronic energy over the whole dyads. Such an effect has been observed in dyads consisting of the same chromophores as here but with a smaller and rigid aromatic bridge.[82] Because of the large coupling, charge separation was ultrafast and solvent-controlled. The peptide linker used here results in a weak coupling that ensures that each chromophoric unit retains its identity and that allows energy and charge transfer processes to take place.

The excited-state dynamics of dyad **1** is strongly solvent-dependent due to the existence of a charge-separated state located below or above the local excited states, depending on the solvent polarity. In an apolar solvent, the most striking feature is the occurrence of excitation energy transfer from the porphyrin on a timescale similar to that of vibrational relaxation, and consequently, it is significantly faster than predicted by Förster theory using thermally equilibrated electronic spectra. Ultimately, the electronic energy ends up on the lowest local triplet excited state. In polar solvents, the excited-state dynamics is shortened by almost 5 orders of magnitude because of the occurrence of charge separation, which totally suppresses the population of the triplet state. As both local singlet excited states are in equilibrium, both electron (excitation on the porphyrin) and hole (excitation on the naphthalenediimide) are probably operative.

Much less solvent dependence is observed with dyad **2**, where charge separation is endergonic and occurs on the same timescale as intersystem crossing. The most striking feature of this dyad is that both singlet and triplet energy transfers are observed and take place in opposite directions. Upon excitation at 600 nm, four different local electronic excited states are consecutively populated with the energy shuttling between the two sides of the dyad. This behavior, due to the very specific location of the excited singlet and triplet states, is quite unusual, and might find some applications in areas such as sensing, molecular electronics, or logics.

ASSOCIATED CONTENT

Supporting Information

Frontier molecular orbitals, transient absorption spectra, distance dependence of the CS rate constant, calculation of the driving force, calculation of the Coulomb interaction energy, details of the synthesis of the arrays, ^{1}H NMR spectra of **5** and **2**, ^{13}C NMR spectra of **5** and **2**, and MALDI mass spectrum of **1**. This material is available free of charge via the Internet at http://pubs.acs.org.

AUTHOR INFORMATION

Corresponding Author

*E-mail: eric.vauthey@unige.ch.

Notes

The authors declare no competing financial interest.

ACKNOWLEDGMENTS

This work was supported by the Swiss National Science Foundation through project nr. 200020-147098 and the University of Geneva, the University of Geneva and the Australian Research Council (S.V.B., Future Fellowship Scheme, FT110100152).

REFERENCES

(1) Sundström, V. Femtobiology. *Annu. Rev. Phys. Chem.* **2008**, *59*, 53−77.

(2) van Grondelle, R.; Novoderezhkin, V. I. Photosynthesis: Quantum Design for a Light Trap. *Nature* **2010**, *463*, 614−615.

(3) Hohmann-Marriott, M. F.; Blankenship, R. E. Evolution of Photosynthesis. *Annu. Rev. Plant Biol.* **2011**, *62*, 515−548.

(4) Gust, D.; Moore, T. A.; Moore, A. L. Solar Fuels via Artificial Photosynthesis. *Acc. Chem. Res.* **2009**, *42*, 1890−1898.

(5) Borgström, M.; Shaikh, N.; Johansson, O.; Anderlund, M. F.; Styring, S.; Aakermark, B.; Magnuson, A.; Hammarström, L. Light Induced Manganese Oxidation and Long-Lived Charge Separation in a Mn2II,II-RuII(bpy)3-Acceptor Triad. *J. Am. Chem. Soc.* **2005**, *127*, 17504−17515.

(6) Wasielewski, M. R. M. Self-Assembly Strategies for Integrating Light Harvesting and Charge Separation in Artificial Photosynthetic Systems. *Acc. Chem. Res.* **2009**, *42*, 1910−21.

(7) Grimm, B.; Schornbaum, J.; Jasch, H.; Trukhina, O.; Wessendorf, F.; Hirsch, A.; Torres, T.; Guldi, D. M. Step-by-Step Self-Assembled Hybrids that Feature Control over Energy and Charge Transfer. *Proc. Natl. Acad. Sci. U.S.A.* **2012**, *109*, 15565−15571.

(8) Pellegrin, Y.; Odobel, F. Molecular Devices Featuring Sequential Photoinduced Charge Separations for the Storage of Multiple Redox Equivalents. *Coord. Chem. Rev.* **2011**, *255*, 2578−2593.

(9) Sazanovich, I. V.; Alamiry, M. A. H.; Best, J.; Bennett, R. D.; Bouganov, O. V.; Davies, E. S.; Grivin, V. P.; Meijer, A. J. H. M.; Plyusnin, V. F.; Ronayne, K. L.; et al. Excited State Dynamics of a PtII Diimine Complex bearing a Naphthalene-Diimide Electron Acceptor. *Inorg. Chem.* **2008**, *47*, 10432−10445.

(10) Bhosale, S.; Sisson, A. L.; Talukdar, P.; Fürstenberg, A.; Banerji, N.; Vauthey, E.; Bollot, G.; Mareda, J.; Röger, C.; Würthner, F.; et al. Photoproduction of Proton Gradients with Pi-Stacked Fluorophore Scaffolds in Lipid Bilayers. *Science* **2006**, *313*, 84−86.

(11) Sakai, N.; Lista, M.; Kel, O.; Sakurai, S.-i.; Emery, D.; Mareda, J.; Vauthey, E.; Matile, S. Self-Organizing Surface-Initiated Polymerization: Facile Access to Complex Functional Systems. *J. Am. Chem. Soc.* **2011**, *133*, 15224−15227.

(12) De Silva, P. A.; Uchiyama, S. Molecular Logic Gates and Luminescent Sensors Based on Photoinduced Electron Transfer. *Top. Curr. Chem.* **2011**, *300*, 1−28.

(13) Tour, J. M. Molecular Electronics. Synthesis and Testing of Components. *Acc. Chem. Res.* **2000**, *33*, 791−804.

(14) Ratner, M. A.; Jortner, J., Molecular Electronics: Some Directions. In *Molecular Electronics*, Ratner, M. A., Jortner, J., Eds. Blackwell Science, Inc.: Oxford, 1997; p 5.

(15) Holten, D.; Bocian, D. F.; Lindsey, J. S. Probing Electronic Communication in Covalently Linked Multiporphyrin Arrays. A Guide to the Rational Design of Molecular Photonics Devices. *Acc. Chem. Res.* **2002**, *35*, 57−69.

(16) Masai, H.; Terao, J.; Seki, S.; Nakashima, S.; Kiguchi, M.; Okoshi, K.; Fujihara, T.; Tsuji, Y. Synthesis of One-Dimensional Metal-Containing Insulated Molecular Wire with Versatile Properties Directed toward Molecular Electronics Materials. *J. Am. Chem. Soc.* **2014**, *136*, 1742−1745.

DOI: 10.1021/jp5108685
J. Phys. Chem. B 2015, 119, 7308−7320

(17) Astruc, D.; Boisselier, E.; Ornelas, C. Dendrimers Designed for Functions: From Physical, Photophysical, and Supramolecular Properties to Applications in Sensing, Catalysis, Molecular Electronics, Photonics, and Nanomedicine. *Chem. Rev.* **2010**, *110*, 1857−1959.
(18) Adams, D. M.; Brus, L.; Chidsey, C. E. D.; Creager, S.; Creutz, C.; Kagan, C. R.; Kamat, P. V.; Lieberman, M.; Lindsay, S.; Marcus, R. A.; et al. Charge Transfer in the Nanoscale: Current Status. *J. Phys. Chem. B* **2003**, *107*, 6668−6697.
(19) Shibano, Y.; Imahori, H.; Sreearunothai, P.; Cook, A. R.; Miller, J. R. Conjugated "Molecular Wire" for Excitons. *J. Phys. Chem. Lett.* **2010**, *1*, 1492−1496.
(20) Lammi, R. K.; Ambroise, A.; Balasubramanian, T.; Wagner, R. W.; Bocian, D. F.; Holten, D.; Lindsey, J. S. Structural Control of Photoinduced Energy Transfer between Adjacent and Distant Sites in Multiporphyrin Arrays. *J. Am. Chem. Soc.* **2000**, *122*, 7579−7591.
(21) Van Patten, P. G.; Shreve, A. P.; Lindsey, J. S.; Donohoe, R. J. Energy-Transfer Modeling for the Rational Design of Multiporphyrin Light-Harvesting Arrays. *J. Phys. Chem. B* **1998**, *102*, 4209−4216.
(22) Peng, X.; Aratani, N.; Takagi, A.; Matsumoto, T.; Kawai, T.; Hwang, I.-W.; Ahn, T. K.; Kim, F.; Osuka, A. A Dodecameric Porphyrin Wheel. *J. Am. Chem. Soc.* **2004**, *126*, 4468−4469.
(23) Aratani, N.; Osuka, A.; Cho, H. S.; Kim, D. Photochemistry of Covalently-Linked Multi-Porphyrinic Systems. *J. Photochem. Photobiol. C* **2002**, *3*, 25−52.
(24) Brodard, P.; Matzinger, S.; Vauthey, E.; Mongin, O.; Papamicaël, C.; Gossauer, A. Investigations of Electronic Energy Transfer Dynamics in Multiporphyrin Arrays. *J. Phys. Chem. A* **1999**, *103*, 5858−5870.
(25) Morandeira, A.; Vauthey, E.; Schuwey, A.; Gossauer, A. Ultrafast Excited State Dynamics of Tri- and Hexaporphyrin Arrays. *J. Phys. Chem. A* **2004**, *108*, 5741−5751.
(26) Yeow, E. K. L.; Ghiggino, K. P.; Reek, J. N. H.; Crossley, M. J.; Bosman, A. W.; Schenning, A. P. H. J.; Meijer, E. W. The Dynamics of Electronic Energy Transfer in Novel Multiporphyrin Functionalized Dendrimers: A Time-Resolved Fluorescence Anisotropy Study. *J. Phys. Chem. B* **2000**, *104*, 2596−2606.
(27) O'Sullivan, M. C.; Sprafke, J. K.; Kondratuk, D. V.; Rinfray, C.; Claridge, T. D. W.; Saywell, A.; Blunt, M. O.; O'Shea, J. N.; Beton, P. H.; Malfois, M.; et al. Vernier Templating and Synthesis of a 12-Porphyrin Nano-Ring. *Nature* **2011**, *469*, 72−75.
(28) Aratani, N.; Kim, D.; Osuka, A. Discrete Cyclic Porphyrin Arrays as Artificial Light-Harvesting Antenna. *Acc. Chem. Res.* **2009**, *42*, 1922−1934.
(29) Imahori, H. Giant Multiporphyrin Arrays as Artificial Light-Harvesting Antennas. *J. Phys. Chem. B* **2004**, *108*, 6130−6143.
(30) Kumble, R.; Palese, S.; Lin, V. S. Y.; Therien, M. J.; Hochstrasser, R. M. Ultrafast Dynamics of Higly Conjugated Porphyrin Arrays. *J. Am. Chem. Soc.* **1998**, *120*, 11489−11498.
(31) Biemans, H. A. M.; Rowan, A. E.; Verhoeven, A.; Vanoppen, P.; Latterini, L.; Foekema, J.; Schenning, A. P. H. J.; Meijer, E. W.; deSchryver, F. C.; Nolte, R. J. M. Hexakis Porphyrinato Benzene. A New Class of Porphyrin Array. *J. Am. Chem. Soc.* **1998**, *120*, 11054−11060.
(32) Kelley, R. F.; Goldsmith, R. H.; Wasielewski, M. R. Ultrafast Energy Transfer within Cyclic Self-Assembled Chlorophyll Tetramers. *J. Am. Chem. Soc.* **2007**, *129*, 6384−6385.
(33) Diring, S.; Puntoriero, F.; Nastasi, F.; Campagna, S.; Ziessel, R. Star-Shaped Multichromophoric Arrays from Bodipy Dyes Grafted on Truxene Core. *J. Am. Chem. Soc.* **2009**, *131*, 6108−6110.
(34) Ziessel, R.; Ulrich, G.; Haefele, A.; Harriman, A. An Artificial Light-Harvesting Array Constructed from Multiple Bodipy Dyes. *J. Am. Chem. Soc.* **2013**, *135*, 11330−11344.
(35) Kaloudi-Chantzea, A.; Karakostas, N.; Pitterl, F.; Raptopoulou, C. P.; Glezos, N.; Pistolis, G. Efficient Supramolecular Synthesis of a Robust Circular Light-Harvesting Bodipy-Dye Based Array. *Chem. Commun.* **2012**, *48*, 12213−12215.
(36) Foster, S.; Finlayson, C. E.; Keivanidis, P. E.; Huang, Y.-S.; Hwang, I.; Friend, R. H.; Otten, M. B. J.; Lu, L.-P.; Schwartz, E.; Nolte, R. J. M.; et al. Improved Performance of Perylene-Based Photovoltaic Cells Using Polyisocyanopeptide Arrays. *Macromolecules* **2009**, *42*, 2023−2030.
(37) Schlosser, F.; Sung, J.; Kim, P.; Kim, D.; Wurthner, F. Excitation Energy Migration in Covalently Linked Perylene Bisimide Macrocycles. *Chem. Sci.* **2012**, *3*, 2778−2785.
(38) Ahrens, M. J.; Sinks, L. E.; Rybtchinski, B.; Liu, W.; Jones, B. A.; Giaimo, J. M.; Gusev, A. V.; Goshe, A. J.; Tiede, D. M.; Wasielewski, M. R. Self-Assembly of Supramolecular Light-Harvesting Arrays from Covalent Multi-Chromophore Perylene-3,4:9,10-bis(dicarboximide) Building Blocks. *J. Am. Chem. Soc.* **2004**, *126*, 8284−8294.
(39) Oesterling, I.; Muellen, K. Multichromophoric Polyphenylene Dendrimers: Toward Brilliant Light Emitters with an Increased Number of Fluorophores. *J. Am. Chem. Soc.* **2007**, *129*, 4595−4605.
(40) Sakai, N.; Sisson, A. L.; Bürgi, T.; Matile, S. Zipper Assembly of Photoactive Rigid-Rod Naphthalenediimide-Stack Architectures on Gold Nanoparticles and Gold Electrode. *J. Am. Chem. Soc.* **2007**, *129*, 15758−15759.
(41) Bhosale, R.; Kishore, R. S. K.; Ravikumar, V.; Kel, O.; Vauthey, E.; Sakai, N.; Matile, S. Zipper Assembly of SHJ Photosystems: Focus on Red Naphthalenediimides, Optoelectronic Finetuning and Topological Matching. *Chem. Sci.* **2010**, *1*, 357−368.
(42) Sakai, N.; Mareda, J.; Vauthey, E.; Matile, S. Core-Substituted Naphthalenediimides. *Chem. Commun.* **2010**, *46*, 4225−4237.
(43) Zieschang, F.; Schmiedel, A.; Holzapfel, M.; Ansorg, K.; Engels, B.; Lambert, C. Solvent Controlled Energy Transfer Processes in Triarylamine-Triazole Based Dendrimers. *J. Phys. Chem. C* **2013**, *117*, 19816−19831.
(44) Vauthey, E. Photoinduced Symmetry-Breaking Charge Separation. *ChemPhysChem* **2012**, *13*, 2001−2011.
(45) Giaimo, J. M.; Gusev, A. V.; Wasielewski, M. R. Excited-State Symmetry Breaking in Cofacial and Linear Dimers of a Green Perylenediimide Chlorophyll Analogue Leading to Ultrafast Charge Separation. *J. Am. Chem. Soc.* **2002**, *124*, 8530−8531.
(46) Holman, M. W.; Yan, P.; Adams, D. M.; Westenhoff, S.; Silva, C. Ultrafast Spectroscopy of the Solvent Dependence of Electron Transfer in a Perylenebisimide Dimer. *J. Phys. Chem. A* **2005**, *109*, 8548−8552.
(47) Banerji, N.; Fürstenberg, A.; Bhosale, S.; Sisson, A. L.; Sakai, N.; Matile, S.; Vauthey, E. Ultrafast Photoinduced Charge Separation in Naphthalene Diimide Based Multichromophoric Systems in Liquid Solutions and in a Lipid Membrane. *J. Phys. Chem. B* **2008**, *112*, 8912−8922.
(48) Whited, M. T.; Djurovich, P. I.; Roberts, S. T.; Durrell, A. C.; Schlenker, C. W.; Bradforth, S. E.; Thompson, M. E. Singlet and Triplet Excitation Management in a Bichromophoric Near-Infrared-Phosphorescent BODIPY-Benzoporphyrin Platinum Complex. *J. Am. Chem. Soc.* **2011**, *133*, 88−96.
(49) Li, F.; Yang, S. I.; Ciringh, Y.; Seth, J.; Martin, C. H., III; Singh, D. L.; Kim, D.; Birge, R. R.; Bocian, D. F.; Holten, D.; Lindsey, J. S. Design, Synthesis and Photodynamics of Light Harvesting Arrays Comprised of a Porphyrin and One, Two or Eight Boron-Dipyrrin Accessory Pigments. *J. Am. Chem. Soc.* **1998**, *120*, 10001−10017.
(50) Iehl, J.; Nierengarten, J.-F.; Harriman, A.; Bura, T.; Ziessel, R. Artificial Light-Harvesting Arrays: Electronic Energy Migration and Trapping on a Sphere and between Spheres. *J. Am. Chem. Soc.* **2012**, *134*, 988−998.
(51) Sautter, A.; Kaletas, B. K.; Schmid, D. G.; Dobrawa, R.; Zimine, M.; Jung, G.; Van Stokkum, I. H. M.; De Cola, L.; Williams, R. M.; Wuerthner, F. Ultrafast Energy-Electron Transfer Cascade in a Multichromophoric Light-Harvesting Molecular Square. *J. Am. Chem. Soc.* **2005**, *127*, 6719−6729.
(52) Uetomo, A.; Kozaki, M.; Suzuki, S.; Yamanaka, K.-i.; Ito, O.; Okada, K. Efficient Light-Harvesting Antenna with a Multi-Porphyrin Cascade. *J. Am. Chem. Soc.* **2011**, *133*, 13276−13279.
(53) D'Souza, F.; Wijesinghe, C. A.; El-Khouly, M. E.; Hudson, J.; Niemi, M.; Lemmetyinen, H.; Tkachenko, N. V.; Zandler, M. E.; Fukuzumi, S. Ultrafast Excitation Transfer and Charge Stabilization in a Newly Assembled Photosynthetic Antenna-Reaction Center Mimic

DOI: 10.1021/jp5108685
J. Phys. Chem. B 2015, 119, 7308−7320

Composed of Boron Dipyrrin, Zinc Porphyrin and Fullerene. *Phys. Chem. Chem. Phys.* **2011**, *13*, 18168−18178.
(54) Röger, C.; Müller, M. G.; Lysetska, M.; Miloslavina, Y.; Holzwarth, A. R.; Würthner, F. Efficient Energy Transfer from Peripheral Chromophores to the Self-Assembled Zinc Chlorin Rod Antenna: A Bioinspired Light-Harvesting System to Bridge the 'Green Gap'. *J. Am. Chem. Soc.* **2006**, *128*, 6542−6543.
(55) Maligaspe, E.; Kumpulainen, T.; Subbaiyan, N. K.; Zandler, M. E.; Lemmetyinen, H.; Tkachenko, N. V.; D'Souza, F. Electronic Energy Harvesting Multi BODIPY-Zinc Porphyrin Dyads Accommodating Fullerene as Photosynthetic Composite of Antenna-Reaction Center. *Phys. Chem. Chem. Phys.* **2010**, *12*, 7434−7444.
(56) Terazono, Y.; Kodis, G.; Liddell, P. A.; Garg, V.; Moore, T. A.; Moore, A. L.; Gust, D. Multiantenna Artificial Photosynthetic Reaction Center Complex. *J. Phys. Chem. B* **2009**, *113*, 7147−7155.
(57) Kodis, G.; Terazono, Y.; Liddell, P. A.; Andréasson, J.; Garg, V.; Hambourger, M.; Moore, T. A.; Moore, A. L.; Gust, D. Energy and Photoinduced Electron Transfer in a Wheel-Shaped Artificial Photosynthetic Antenna-Reaction Center Complex. *J. Am. Chem. Soc.* **2006**, *128*, 1818−1827.
(58) D'Souza, F.; Smith, P. M.; Zandler, M. E.; McCarty, A. L.; Itou, M.; Araki, Y.; Ito, O. Energy Transfer Followed by Electron Transfer in a Supramolecular Triad Composed of Boron Dipyrrin, Zinc Porphyrin, and Fullerene: A Model for the Photosynthetic Antenna-Reaction Center Complex. *J. Am. Chem. Soc.* **2004**, *126*, 7898−7907.
(59) Guldi, D. M. Fullerene-Porphyrin Architecture; Photosynthetic Antenna and Reaction Center Model. *Chem. Soc. Rev.* **2002**, *31*, 22−36.
(60) Kuclauskas, D.; Liddell, P. A.; Lin, S.; Johnson, T. E.; Weghorn, S. J.; Lindsey, J. S.; Moore, A. L.; Moore, T. A.; Gust, D. An Artificial Photosynthetic Antenna-Reaction Center Complex. *J. Am. Chem. Soc.* **1999**, *121*, 8604−8614.
(61) Gust, D.; Moore, T. A.; Moore, A. L.; Macpherson, A. N.; Lopez, A.; DeGraziano, J. M.; Gouni, I.; Bittersmann, E.; Seely, G. R.; et al. Photoinduced Electron and Energy Transfer in Molecular Pentads. *J. Am. Chem. Soc.* **1993**, *115*, 11141−11152.
(62) Palacios, R. E.; Kodis, G.; Gould, S. L.; de la Garza, L.; Brune, A.; Gust, D.; Moore, T. A.; Moore, A. L. Artificial Photosynthetic Reaction Centers: Mimicking Sequential Electron and Triplet-Energy Transfer. *ChemPhysChem* **2005**, *6*, 2359−2370.
(63) Brown, K. E.; Veldkamp, B. S.; Co, D. T.; Wasielewski, M. R. Vibrational Dynamics of a Perylene−Perylenediimide Donor−Acceptor Dyad Probed with Femtosecond Stimulated Raman Spectroscopy. *J. Phys. Chem. Lett.* **2012**, *3*, 2362−2366.
(64) Banerji, N.; Duvanel, G.; Perez-Velasco, A.; Maity, S.; Sakai, N.; Matile, S.; Vauthey, E. Excited-State Dynamics of Hybrid Multichromophoric Systems: Toward an Excitation Wavelength Control of the Charge Separation Pathways. *J. Phys. Chem. A* **2009**, *113*, 8202−8212.
(65) Bandi, V.; El-Khouly, M. E.; Ohkubo, K.; Nesterov, V. N.; Zandler, M. E.; Fukuzumi, S.; D'Souza, F. Excitation-Wavelength-Dependent, Ultrafast Photoinduced Electron Transfer in Bisferrocene/BF2-Chelated-Azadipyrromethene/Fullerene Tetrads. *Chem.—Eur. J.* **2013**, *19*, 7221−7230.
(66) Lembo, A.; Tagliatesta, P.; Guldi, D. M.; Wielopolski, M.; Nuccetelli, M. Porphyrin/Oligo-Ethynylenephenylene/Fullerene Triads: Synthesis and Electrochemical and Photophysical Characterization of the New Porphyrin-Oligo-PPE-Fullerene Systems. *J. Phys. Chem. A* **2009**, *113*, 1779−1793.
(67) Villamaina, D.; Kelson, M. M. A.; Bhosale, S. V.; Vauthey, E. Excitation Wavelength Dependence of the Charge Separation Pathways in Tetraporphyrin-Naphthalene Diimide Pentads. *Phys. Chem. Chem. Phys.* **2014**, *16*, 5188−5200.
(68) Gao, J.; Müller, P.; Wang, M.; Eckhardt, S.; Lauz, M.; Fromm, K. M.; Giese, B. Electron Transfer in Peptides: The Influence of Charged Amino Acids. *Angew. Chem., Int. Ed.* **2011**, *50*, 1926−1930.
(69) Shin, Y.-g. K.; Newton, M. D.; Isied, S. S. Distance Dependence of Electron Transfer Across Peptides with Different Secondary Structures: The Role of Peptide Energetics and Electronic Coupling. *J. Am. Chem. Soc.* **2003**, *125*, 3722−3732.
(70) Gao, X.; Qiu, W.; Yang, X.; Liu, Y.; Wang, Y.; Zhang, H.; Qi, T.; Liu, Y.; Lu, K.; Du, C.; et al. First Synthesis of 2,3,6,7-Tetrabromonaphthalene Diimide. *Org. Lett.* **2007**, *9*, 3917−3920.
(71) Luguya, R.; Jaquinod, L.; Fronczek, F. R.; Vicente, M. G. H.; Smith, K. M. Synthesis and Reactions of Meso-(p-Nitrophenyl)-Porphyrins. *Tetrahedron* **2004**, *60*, 2757−2763.
(72) Muller, P.-A.; Högemann, C.; Allonas, X.; Jacques, P.; Vauthey, E. Deuterium Isotope Effect on the Charge Recombination Dynamics of Contact Ion Pairs Formed by Electron Transfer Quenching in Acetonitrile. *Chem. Phys. Lett.* **2000**, *326*, 321−327.
(73) Fürstenberg, A.; Vauthey, E. Excited State Dynamics of the Fluorescent Probe Lucifer Yellow in Liquid Solutions in in Heterogeneous Media. *Photochem. Photobiol. Sci.* **2005**, *4*, 260−267.
(74) Morandeira, A.; Engeli, L.; Vauthey, E. Ultrafast Charge Recombination of Photogenerated Ion Pairs to an Electronic Excited State. *J. Phys. Chem. A* **2002**, *106*, 4833−4837.
(75) Duvanel, G.; Grilj, J.; Chaumeil, H.; Jacques, P.; Vauthey, E. Ultrafast Excited-State Dynamics of a Series of Zwitterionic Pyridinium Phenoxides with Increasing Sterical Hindering. *Photochem. Photobiol. Sci.* **2010**, *9*, 908−915.
(76) Duvanel, G.; Banerji, N.; Vauthey, E. Excited-State Dynamics of Donor-Acceptor Bridged Systems Containing a Boron-Dipyrromethene Chromophore: Interplay between Charge Separation and Reorientational Motion. *J. Phys. Chem. A* **2007**, *111*, 5361−5369.
(77) Lang, B.; Mosquera-Vazquez, S.; Lovy, D.; Sherin, P.; Markovic, V.; Vauthey, E. Broadband Ultraviolet-Visible Transient Absorption Spectroscopy in the Nanosecond to Microsecond Time Domain with Sub-Nanosecond Time Resolution. *Rev. Sci. Instrum.* **2013**, *84*, 073107−073108.
(78) Perdew, J. P. Density-Functional Approximation for the Correlation Energy of the Inhomogeneous Electron Gas. *Phys. Rev. B* **1986**, *33*, 8822−8824.
(79) Bauernschmitt, R.; Ahlrichs, R. Treatment of Electronic Excitations within the Adiabatic Approximation of Time Dependent Density Functional Theory. *Chem. Phys. Lett.* **1996**, *256*, 454−464.
(80) Frisch, M. J.; Trucks, G. W.; Schlegel, H. B.; Scuseria, G. E.; Robb, M. A.; Cheeseman, J. R.; Scalmani, G.; Barone, V.; Mennucci, B.; Petersson, G. A., et al. *Gaussian 09*, revision C1; Gaussian, Inc.: Wallingford, CT, 2010.
(81) Eng, M. P.; Ljungdahl, T.; Mårtensson, J.; Albinsson, B. Triplet Excitation Energy Transfer in Porphyrin-Based Donor−Bridge−Acceptor Systems with Conjugated Bridges of Varying Length: An Experimental and DFT Study. *J. Phys. Chem. B* **2006**, *110*, 6483−6491.
(82) Banerji, N.; Bhosale, S. V.; Petkova, I.; Langford, S. J.; Vauthey, E. Ultrafast Excited-State Dynamics of Strongly Coupled Porphyrin/Core-Substituted-Naphthalenediimide Dyads. *Phys. Chem. Chem. Phys.* **2011**, *13*, 1019−1029.
(83) Pigliucci, A.; Duvanel, G.; Daku, L. M. L.; Vauthey, E. Investigation of the Influence of Solute-solvent Interactions on the Vibrational Energy Relaxation Dynamics of Large Molecules in Liquids'. *J. Phys. Chem. A* **2007**, *111*, 6135−6145.
(84) Yu, H.-Z.; Baskin, J. S.; Zewail, A. H. Ultrafast Dynamics of Porphyrins in the Condensed Phase: II. Zinc Tetraphenylporphyrin. *J. Phys. Chem. A* **2002**, *106*, 9845−9854.
(85) Liu, X.; Tripathy, U.; Bhosale, S. V.; Langford, S. J.; Steer, R. P. Photophysics of Soret-Excited Tetrapyrroles in Solution. II. Effects of Perdeuteration, Substituent Nature and Position, and Macrocycle Structure and Conformation in Zinc(II) Porphyrins. *J. Phys. Chem. A* **2008**, *112*, 8986−8998.
(86) Cho, H. S.; Jeong, D. H.; Yoon, M.-C.; Kim, Y. H.; Kim, Y.-R.; Kim, D.; Jeoung, S. C.; Kim, S. K.; Aratani, N.; Shinmori, H.; et al. Excited-State Energy Transfer Processes in Phenylene- and Biphenylene-Linked and Directly-Linked Zinc(II) and Free-Base Hybrid Diporphyrins. *J. Phys. Chem. A* **2001**, *105*, 4200−4210.
(87) Villamaina, D.; Bhosale, S.; Langford, S. J.; Vauthey, E. Excited-State Dynamics of Porphyrin-Naphthalenediimide-Porphyrin Triads. *Phys. Chem. Chem. Phys.* **2013**, *15*, 1177−1187.

DOI: 10.1021/jp5108685
J. Phys. Chem. B 2015, 119, 7308−7320

(88) Ohno, O.; Kaizu, Y.; Kobayashi, H. Luminescence of some Metalloporphins Including the Complexes of the IIIb Metal Group. *J. Chem. Phys.* **1985**, *82*, 1779−1787.
(89) Baskin, J. S.; Yu, H.-Z.; Zewail, A. H. Ultrafast Dynamics of Porphyrins in the Condensed Phase: I. Free Base Tetraphenylporphyrin. *J. Phys. Chem. A* **2002**, *106*, 9837−9844.
(90) Grilj, J.; Laricheva, E. N.; Olivucci, M.; Vauthey, E. Fluorescence of Radical Ions in Liquid Solution: Wurster's Blue as a Case Study. *Angew. Chem., Int. Ed.* **2011**, *50*, 4496−4498.
(91) Grilj, J.; Zonca, C.; Daku, L. M. L.; Vauthey, E. Photophysics of the Galvinoxyl Free Radical Revisited. *Phys. Chem. Chem. Phys.* **2012**, *14*, 6345−6351.
(92) van Stokkum, I. H. M.; Larsen, D. S.; van Grondelle, R. Global and Target Analysis of Time-Resolved Spectra. *Biochim. Biophys. Acta, Bioenerg.* **2004**, *1657*, 82−104.
(93) Rosspeintner, A.; Lang, B.; Vauthey, E. Ultrafast Photochemistry in Liquids. *Annu. Rev. Phys. Chem.* **2013**, *64*, 247−271.
(94) Okhrimenko, A. N.; Gusev, A. V.; Rodgers, M. A. J. Excited State Relaxation Dynamics of the Zinc(II) Tetraphenylporphine Cation Radical. *J. Phys. Chem. A* **2005**, *109*, 7653−7656.
(95) Petersson, J.; Eklund, M.; Davidsson, J.; Hammarström, L. Ultrafast Electron Transfer Dynamics of a Zn(II)porphyrin/Viologen Complex Revisited: S2 vs S1 Reactions and Survival of Excess Excitation Energy. *J. Phys. Chem. B* **2010**, *114*, 14329−14338.
(96) Högemann, C.; Vauthey, E. Investigation of the Competition between Electron and Energy Transfer in the Quenching of Aromatic Ketones in the Triplet State Using Picosecond Transient Grating Spectroscopy. *J. Phys. Chem. A* **1998**, *102*, 10051−10059.
(97) Gosztola, D.; Niemczik, M. P.; Svec, W.; Lukas, A. S.; Wasielewski, M. R. Excited Doublet States of Electrochemically Generated Aromatic Imide and Diimide Radical Anions. *J. Phys. Chem. A* **2000**, *104*, 6545−6551.
(98) Pineiro, M.; Carvalho, A. L.; Pereira, M. M.; Gonsalves, A. M. d. A. R.; Arnaut, L. G.; Formosinho, S. J. Photoacoustic Measurements of Porphyrin Triplet-State Quantum Yields and Singlet-Oxygen Efficiencies. *Chem.—Eur. J.* **1998**, *4*, 2299−2307.
(99) Weller, A. Photoinduced Electron Rransfer in Solutions: Exciplex and Radical Ion Pair Formation Free Enthalpies and their Solvent Dependence. *Z. Phys. Chem. N.F.* **1982**, *133*, 93−98.
(100) Förster, T. Intermolecular energy transfer and fluorescence. *Ann. Physik* **1948**, *2*, 55−75.
(101) Dexter, D. L. A Theory of Sensitized Luminescence in Solids. *J. Chem. Phys.* **1953**, *21*, 836−850.
(102) Pullerits, T.; Hess, S.; Herek, J. L.; Sundström, V. Temperature Dependence of Excitation Transfer in LH2 of Rhodobacter Sphaeroides. *J. Phys. Chem. B* **1997**, *101*, 10560−10567.
(103) Perrin, M. H.; Gouterman, M.; Perrin, C. L. Vibronic Coupling. VI. Vibronic Borrowing in Cyclic Polyenes and Porphyrin. *J. Chem. Phys.* **1969**, *50*, 4137−4150.
(104) Closs, G. L.; Johnson, M. D.; Miller, J. R.; Piotrowiak, P. A Connection between Intramolecular Long-Range Electron, Hole and Triplet Energy Transfer. *J. Am. Chem. Soc.* **1989**, *111*, 3751−3753.

DOI: 10.1021/jp5108685
J. Phys. Chem. B 2015, 119, 7308−7320